NASA Technical Memorandum 81596

Heat Transfer Coefficients for Staggered Arrays of Short Pin Fins

G. James VanFossen
Lewis Research Center
Cleveland, Ohio

Prepared for the
Twenty-sixth Annual International Gas Turbine Conference
sponsored by the American Society of Mechanical Engineers
Houston, Texas, March 8-12, 1981

NASA

HEAT TRANSFER COEFFICIENTS FOR STAGGERED ARRAYS OF SHORT PIN FINS

by G. James VanFossen

National Aeronautics and Space Administration
Lewis Research Center
Cleveland, Ohio

NOMENCLATURE

$\bar{A}$	average flow area in test section, V/L
A_p	cross sectional area of a pin, $\pi D_o^2/4$
A_w	endwall area defined by equation (11)
D'	characteristic length of test section
D_o	pin diameter
H	height of plain channel
$\bar{h}$	average heat transfer coefficient in pin fin test section
h_{eff}	effective heat transfer coefficient as defined by equation (6)
$\bar{h}_p$	average heat transfer coefficient on pin surface
$\bar{h}_w$	average heat transfer coefficient on endwall surface
k_a	thermal conductivity of air evaluated at T_r
k_p	thermal conductivity of pin material
L	length of heated portion of test section in flow direction
ℓ	pin half length used in equation (9)
m	fin parameter defined by equation (13)
N_L	number of pin rows in flow direction
N_T	number of pins in a row transverse to flow direction
Nu	Nusseit number, $\bar{h}D'/k_a$
P	pin perimeter, πD_o
Pr	Prandtl number of air
Q	heat dissipated in electric heater
Q_{loss}	heat lost to surroundings from test section
r	recovery factor
Re	Reynolds number, $(\dot{w}/\bar{A})D'/\mu$
S	total heat transfer surface area
S_h	surface area of heaters
T_a	ambient air temperature
T_{aw}	adiabatic wall temperature
T_r	reference temperature defined by equation (5)
T_s	air static temperature
T_w	endwall temperature
U	overall heat transfer coefficient for heat loss from test section to surroundings
V	open volume in test section
W	width of plain channel

$\dot{w}$	mass flow rate
X	ratio of heat transfer coefficient on pin surface to that on the endwall, h_p/h_w
x_S	ratio of pin height to pin diameter
x_T	ratio of pin spacing to pin diameter
θ	pin angle of inclination measured from normal to endwall
μ	viscosity of air

INTRODUCTION

In designing the cooling configuration for a turbine blade, many heat transfer augmentation schemes are available; film cooling, internal impingement, boundary layer trip strips, and various types of fins are a few of the popular ones. In the trailing edge region, however, aerodynamic considerations demand a small wedge angle for the blade profile. As a result the internal passages become so narrow that the choice of cooling scheme is limited. Pin fins are one augmentation device that can be used to increase heat transfer in this region. Pin fins at the trailing edge also serve a structural purpose by holding the suction and pressure surfaces of the blade together. The pin fins of interest here are circular cylinders that span the distance between the suction and pressure surfaces which form the endwalls of the cooling passage. Heat from the hot gas stream passes through the endwalls and is conducted along the pins and convected to the cooling air. Heat is also convected to the cooling air from the endwalls between the pins.

Due mainly to limits in casting technology, pin fins cannot be reliably made much smaller than about 1 millimeter (0.04 in.) in diameter. This means that in the narrow trailing edge of most turbine blades the pins may be relatively "short" (less than about four diameters in length). In some cases, the addition of pins to the cooling passage may actually cover up more wall surface area than they add in pin surface area; thus, the terms fin or extended surface do not really apply in the literal sense. One of the main functions of the pins in the turbine cooling application is to increase the level of turbulence in the cooling flow rather than add heat transfer surface area.

There are no data for short pin fins of the type used in turbine blade cooling available in the literature. Data for both in-line and staggered arrays of pin fins are given in references 1 to 5. The data in these references were taken by people interested in high efficiency, compact heat exchangers. To keep heat transfer effectiveness high, the configurations they tested all contained relatively long pins; the shortest were four diameters in length. These pins are long compared to those used in many cooled turbine blades. In references 4 and 5, both staggered and in-line arrays of pin fins were investigated but the pins did not extend entirely across the passage.

Heat exchangers usually contain many rows of pins in the streamwise direction. The flow and heat transfer are said to be "fully developed" for more than about eight rows of pins; that is, the heat transfer coefficient changes rapidly in the first few rows and then remains relatively constant in the downstream direction. Thus the average heat transfer coefficient for the case of only a few rows will be different than that for "fully developed" flow. Due to the limited space available, the turbine blade cooling application does not allow a large number of rows to be used, and again one can see that another type of data is required by the turbine blade designer.

Another possible source of heat transfer data is the extensive literature on heat transfer to tube banks. Examples of these are found in references 1, 6, and 7. Tube banks resemble long pin fins. There are two major differences, however, between the pin fins of interest here and tube banks. One difference is that no endwalls are present for tube banks; a large portion of the heat transfer is known to be through the endwalls for the turbine cooling application. The other difference is in the boundary conditions. For the turbine application or for compact heat exchanger application, heat is conducted along the pin and is convected from both endwall and pin surfaces; this results in a significant temperature gradient along the pin. Tube banks usually have fluid flowing in the tubes; heat is conducted through the tube wall and is then convected from the tube surface. The tube walls are thus nearly isothermal in the direction of the tube axis. The application of tube bank data to turbine blade cooling is therefore questionable.

The objective of this study was to obtain heat transfer data for staggered arrays of short pin fins in order to determine if data available in the literature can be applied to turbine blade cooling. Heat transfer coefficients on both the pins and the endwalls were obtained for four pin fin surfaces. Two different model geometries were used in the present study. The larger model had 0.635-centimeter-(0.25-in.-) diameter pins which were spaced four diameters apart in an equilateral triangular array. The pins for this model were two diameters long. Three variations of this model were tested; one had copper pins that were perpendicular to the endwalls, another had wooden pins that were perpendicular to the endwalls and the third had copper pins that were inclined to the endwalls. The smaller test section had copper pins that were 0.3175 centimeter (0.125 in.) in diameter and spaced two diameters apart; the pin height of the smaller model was 0.5 diameter. All pin fin configurations tested had four rows of pins in the flow direction. Two plain channel (no pin fins) configurations were also tested to check the accuracy of the data by comparing the heat transfer results with an accepted correlation for flow in a duct. Reynolds numbers ranged from 300 to nearly 60 000 which is sufficient to cover the range of interest for the turbine cooling application. Heat transfer data are presented as Nusselt number versus Reynolds number. The wooden pins were used to determine the ratio of heat convected from the pins to heat convected from the endwalls. The inclined pins were tested to determine if they would increase the heat transfer rate over that of perpendicular pins. The pin fin heat transfer data from the present study were compared to data for longer pins and an existing correlation that contains terms to account for the range of pin lengths and pin spacings of interest in turbine cooling.

APPARATUS

A layout of the rig used in the pin fin experiments is shown in Fig. 1. Room air enters the test section through a constant acceleration inlet, passes through one of two turbine flow meters,

through the flow control valves and exits to the building altitude exhaust system. Temperatures were measured with Chromel-Alumel thermocouples referenced to a 339 K (150° F) oven. Pressures were measured with a microprocessor-controlled pressure scanning system similar to the one described in reference 8. Volumetric flow rates were measured with turbine-type flow meters; mass flows were calculated by multiplying volumetric flow rates by the density of the air at the exit of the turbine meter. Density was calculated from the perfect gas law for air using the measured temperature and pressure at the turbine meter exit. All data were converted to engineering units and recorded with the laboratory data acquisition system (ref. 9).

Fig. 2 shows the test section assembly used for the large plain channel and large pin fin models. The inlet bellmouth was covered with 150 grit silicon carbide sandpaper and had a 0.519-centimeter-(0.0625-in.-) diameter trip wire to ensure turbulent flow in the test section. Immediately downstream of the inlet there were three thermocouples to read the inlet air total temperature. Three thermocouples measured the outlet total temperature. During the tests, the whole assmebly was wrapped with a thick blanket of fiberglass insulation to minimize heat loss.

TEST SPECIMENS

Fig. 3 shows the geometry for the perpendicular pin fin test sections. The dimensions and pin spacings are given in Table I. Fig. 4 shows the construction of the flow channel for the large pin fin model. The endwalls that formed the top and bottom of the flow channel were constructed of 0.635-centimeter (0.25-in.) copper plate. The pins were inserted into holes drilled in each plate and soft soldered in place. The solder formed very small fillets between the plate and pins. Pins cast into a turbine blade will probably have much larger fillets. No attempt was made to simulate these larger fillets. The sides of the flow channel were machined from a cloth-reinforced phenolic plastic. The sides were held in place by bolts which extended through the copper plates and phenolic material. The assembly was sealed from air leakage with a silicone rubber sealant.

Thermocouples to measure the endwall temperature were inserted into holes drilled in the edge of each plate. The thermocouples can be seen at the right of Fig. 4. Five thermocouples were used in each plate. Commercially available metal foil electric heaters encased in a polymide base film were attached to the endwalls with a pressure sensitive adhesive. The heater leads can be seen at the left side of Fig. 4.

The test section with wooden pins was made with 0.635-centimeter (0.25-in.) copper plates as endwalls with birch dowels epoxied between the endwalls to form the pins. The endwalls were not drilled to accommodate the wooden pins. A slightly larger fillet was formed between the pins and the endwalls by the epoxy than was formed by the solder used on the copper pins.

The inclined pin fin test section was constructed in a fashion similar to that of the other models with copper pins but the pins were inclined to the endwalls. The angle of inclination was arbitrarily selected as 30° from a normal to the surface of the endwalls. This angle is measured in a plane perpendicular to the flow direction and alternates between positive and negative with successive rows in the streamwise direction. Fig. 5 is a photograph of the inclined pin test section. The pins were set in a staggered array at the endwalls (not an equilateral triangular array) but because successive rows cross at mid-span they give the appearance of an in-line array when viewed in the streamwise direction.

The small pin fin test section was constructed in a fashion similar to the large test section with the exception of the pin spacing and pin lengths. Dimensions for this test section are also given in Table I. Only one thermocouple was installed in each top and bottom endwall plates due to size limitation.

In both the large and small pin fin test sections there were four rows of pins in the streamwise direction. In both models the number of pins in each of the four row alternated between four and five. The first row contained five, the second four, and so on.

Fig. 6 shows the geometry of the plain channel test specimens. Two different size plain channels (corresponding to the two sizes of pin fin test sections) were tested. The dimensions of the plain channels are given in Table II. Construction was the same as the pin fin models but the pins were left out.

TEST PROCEDURE

Heat Loss Calibration

Before any heat transfer data could be analyzed, the heat loss to the surroundings had to be measured. To accomplish this, a series of calibration runs were made with no airflow through the test section. The flow channel was sealed off to minimize natural convection during these tests. Heater power was set at a level that would produce approximately the plate temperature of interest. The rig was then allowed to come to equilibrium which usually took 12 to 14 hours. When a steady plate temperature was reached, power level, plate temperature and ambient air temperature were measured so that an overall loss heat transfer coefficient could be calculated.

Data Runs

Before a data run was made, the electric heaters were used to bring the endwall plate temperature up to the desired value with no airflow through the test section. Plate temperatures were set at an average 21 K (38° F) above ambient air temperature. This value was high enough to allow good accuracy in the measured temperature difference between plate and air and low enough to minimize thermal property variations in the test section. Once the insulation reached approximate equilibrium, the air flow was set to the desired value. Heater power was then adjusted to maintain the plate temperature. When it was certain that equilibrium was attained, five samples of all the data channels were recorded for processing.

DATA ANALYSIS

This section describes how the heat transfer and flow data were reduced to dimensionless form.

Heat Loss

The overall loss heat transfer coefficient U is defined as

$$U = \frac{Q_{loss}}{S_h(T_w - T_a)} \quad (1)$$

This overall loss coefficient was calculated for a range of endwall plate to air temperature differences. A typical plot of the loss coefficient versus endwall plate-to-air temperature difference is shown in Fig. 7. The loss coefficient is a weak function of temperature difference. Once the plate and air temperature are known, Fig. 7 and equation (1) can be used to calculate the heat loss from the test section for the purpose of data analysis.

Reynolds Number

The Reynolds number for all test sections was calculated from the following equation:

$$Re = \frac{(\dot{w}/\bar{A})D'}{\mu} \quad (2)$$

The characteristic length D' was defined as

$$D' = \frac{4V}{S} \quad (3)$$

Note that for the plain channel this reduces to the classical definition of hydraulic diameter for a closed channel. The average flow area is defined by

$$\bar{A} = \frac{V}{L} \quad (4)$$

The viscosity was evaluated at the Eckert reference temperature (ref. 10)

$$T_r = 0.5\ T_w + 0.28\ T_s + 0.22\ T_{aw} \quad (5)$$

Heat Transfer Coefficients

The effective heat transfer coefficient for all test sections was calculated from

$$h_{eff} = \frac{Q - Q_{loss}}{S_h(T_w - T_{aw})} \quad (6)$$

The adiabatic wall temperatures used in equations (5) and (6) were calculated from the following equation:

$$T_{aw} = T_s + r(T_t - T_s) \quad (7)$$

where r is the recovery factor. The total and static temperatures, T_t and T_s, respectively, were determined by solving the one-dimensional momentum and energy equations for the pressures and temperatures in the channel. From tests conducted with no heat flow at high test section Mach numbers it was determined that the best value of recovery factor was

$$r = \sqrt{Pr} \quad (8)$$

The cross-sectional area used for the pin fin portion of the flow model was the minimum free flow area. This value gave the best adiabatic wall temperature and pressure drop results.

Equation (6) gives the heat transfer coefficient which includes the effects of pin efficiency. To find the average heat transfer coefficients on the pin and endwall surface, the heat lost by a plain surface with a heat transfer coefficient of h_{eff} was equated to the heat lost by the pin finned surface. The resulting transcendental equation is then

$$\bar{h}_w\left(1 - \frac{A_p}{A_w \cos\theta}\right) + \frac{\sqrt{PX\bar{h}_w k_p A_p}}{A_w} \tanh\left(\frac{m\ell}{\cos\theta}\right) - h_{eff} = 0 \quad (9)$$

For each h_{eff} measured, equation (9) was solved for the root h_w by the Newton-Raphson iteration technique. In equation (9), A_p is the cross-sectional area of a pin defined by

$$A_p = \frac{\pi}{4} D_o^2 \quad (10)$$

A_w is the area of the endwall associated with one half pin

$$A_w = \frac{\sqrt{3}}{2} (x_T D_o)^2 \quad (11)$$

P is the perimeter of the pin

$$P = \pi D_o \quad (12)$$

The fin parameter m is given by

$$m = \sqrt{\frac{X\bar{h}_w P}{k_p A_p}} \quad (13)$$

where X is the ratio of heat transfer coefficient on the pin surface to that on the endwall surface.

Nusselt Number

The Nusselt number was calculated from the average heat transfer coefficient as

$$Nu = \frac{\bar{h}D'}{k_a} \quad (14)$$

where $\bar{h}$ is the heat transfer coefficient on the pin and endwall surfaces ($X = 1.0$ in eq. (9)). The thermal conductivity of air was evaluated at the reference temperature defined by equation (5).

Thermal Properties

The viscosity and thermal conductivity of air were determined from curve fits of data given in reference 11. The thermal conductivity of the copper used was 3.46 W/cm·K (200 Btu/hr·ft·°F). The thermal conductivity used for the wooden pins was 0.0035 W/cm·K (0.2 Btu/hr·ft·°F).

RESULTS AND DISCUSSION

Fig. 8 is a comparison of both the large and small plain channel heat transfer results with a correlation for turbulent heat transfer in a duct. The correlation has been modified for entrance length effects. The correlation is from reference 12 and the entrance length correction was taken from reference 13. The modified correlation used was

$$Nu = 0.023\, Re^{0.8}\, Pr^{1/3} \left\{ 1.11 \left[\frac{Re^{0.2}}{(L/D')^{0.8}} \right]^{0.275} \right\} \quad (15)$$

For Reynolds numbers above 6000, the agreement between the modified correlation and the experimental data is very good. This good agreement gave confidence that the measurement technique and the data analysis were working well. Below Reynolds numbers of 6000, the agreement is not good. Data for the large and small models are not consistent. This disagreement is thought to be due to differences in the inlets of the two models. The large model had sandpaper and a trip wire at the inlet while the small model did not. In any case, only data in the turbulent range is of interest here because, with pin fins in place, the flow in the test section cannot be laminar and, therefore, inlet treatment is not thought to be important.

It should be noted that two levels of maximum Mach number were obtained in the tests. In the large models (both plain channel and pin fin) the highest Mach number reached was about 0.3, while in the small models the flow was choked at the highest Reynolds number. From Fig. 8 the agreement at high Reynolds numbers for both models indicates that Mach number is not a significant parameter if the data are analyzed as indicated in the previous section.

Fig. 9 is a plot of the short pin fin heat transfer results along with those from other pin fin references. The plain channel data are also replotted on this figure for comparison purposes. The meaning of the letters used for plotting symbols can be found in Table I. When examining the figure, three things become obvious; one is that data from all four configurations tested fall on a single correlating line when the Reynolds and Nusselt numbers are defined as explained in the Data Analysis Section. A least-squares curve fit of all the short pin fin data is

$$Nu = 0.153\, Re^{0.685} \quad (16)$$

The reader is cautioned that this good correlation of data may be fortuitous as only two different geometries were tested. Another conclusion that can be drawn from the figure is that the heat transfer data for short pins are lower than for data found in the literature for longer pins. The third conclusion is that short pin fin heat transfer is about a factor of two higher than that for a plain channel with no fins.

The results shown in Fig. 9 were all obtained using equation (9) with X set equal to 1 to determine $\bar{h}$, the average heat transfer coefficient on the pin and endwall surface. This was done to facilitate comparison with data from the literature where it was assumed that $X = 1$. Data from the test section with wooden pins was used to obtain an estimate of the actual value of X. If equation (9) is applied to the large copper and wooden pin test sections, two independent equations result. The geometries of these two test sections were the same; the only difference was the thermal conductivity of the pins. Experimental data for h_{eff} from both the large copper and the wood pin test sections were curve fit as a function of Reynolds number. At any given Reynolds number the heat transfer coefficient $\bar{h}_w$ was assumed to be the same for both copper and wood test sections because their geometry was identical. For each of a series of Reynolds numbers that covered the range of data, the best value of $\bar{h}_w$ was found by minimizing the difference between the curve fit of experimental data and the value of h_{eff} calculated from equation (9) for both copper and wooden pins. Fig. 10(a) shows a comparison of calculated and measured h_{eff} using $X = 1.0$ for both the copper and wooden pin test sections. From this figure it can be concluded that $X = 1.0$ is not the correct value.

The best value of X for the range of Reynolds numbers of interest was estimated using the method of least squares. Fig. 10(b) shows the comparison between measured and calculated values of h_{eff} using the best estimate $X = 1.345$. Agreement between calculated and measured values is much better. It can be concluded from this analysis that the average heat transfer coefficient on the pin surface is about 35 percent larger than that on the endwalls.

In an effort to increase the average heat transfer coefficient on the pin surface, the inclined pins described previously were tested. It was hoped that the wake shed from a row of inclined pins would be stretched across the next downstream row of pins inclined at the opposite angle and thus be intensified. Inclined pins were found, instead, to give the same average heat transfer coefficient as the perpendicular pins. However, the effective heat transfer can be increased by inclining the pins because of the added pin surface area. Fig. 11 shows the calculated benefit of inclining the pins. The ordinate is the ratio of calculated effective heat transfer coefficient for inclined pins to that for pins perpendicular to the endwalls. The effective heat transfer coefficients were obtained from equation (9) using equations (14) and (16) to find the average heat transfer coefficient $\bar{h}$. For these calculations X was set equal to unity. Pin thermal conductivity was set to 0.26 W/cm·K (15 Btu/hr·ft·°F); this value is representative of the thermal conductivity of the nickel-based superalloys used in turbine blades. Pin spacing was four pin diameters and the distance between the endwalls was two diameters. Effective heat transfer coefficient is seen to increase with pin angle and the increase is greater at the low Reynolds numbers. At a Reynolds number of 500 the effective heat transfer for pins angled at 60° is nearly 50 percent greater than that for perpendicular pins.

A correlation of pin fin heat transfer data that was derived from data available in the literature for pin fins and tube banks is presented in reference 14. The correlation contains terms to account for pin length and spacing. Fig. 12 is a comparison of the heat transfer data from this study with this correlation. It can be concluded from the figure that the correlation does not adequately represent the data for short pin fins.

SUMMARY OF RESULTS

The results of this experimental investigation into the heat transfer characteristics of short, staggered pin fin arrays over a Reynolds number range from 300 to nearly 60,000 can be summarized as follows:

1. Heat transfer for short pin fins was found to be lower than data available in the literature for longer pins.
2. Heat transfer data for both pin fin configurations tested in this study fell on a single correlating line.
3. Heat transfer coefficients on the pin surface were estimated to be about 35 percent higher than those on the endwalls.

4. Inclined pins had the same average heat transfer coefficient as the pins that were perpendicular to the endwalls. It was shown analytically that increasing the pin surface area by inclining the pins can be used to increase the effective heat transfer. This increase was the greatest at the low Reynolds numbers.

5. Short pin fin heat transfer coefficients were significantly higher than those for a plain channel with no pins.

6. An existing correlation for pin fin heat transfer which contains terms to account for the effect of pin length does not adequately represent heat transfer data for short pins.

REFERENCES

1 Kays, W. M., and London, A. L., Compact Heat Exchangers, National Press, Palo Alto, Calif., 1955.

2 Theoclitus, G., "Heat-Transfer and Flow Friction Characteristics of Nine Pin-Fin Surfaces," Journal of Heat Transfer, Vol. 88, Nov. 1966, pp. 385-390.

3 Norris, R. H., and Spofford, W. A., "High Performance Fins for Heat Transfer," Transactions of the ASME, Vol. 64, 1942, pp. 489-496.

4 Sparrow, E. M., and Ramsey, J. W., "Heat Transfer and Pressure Drop for a Staggered Wall-Attached Array of Cylinders with Tip Clearance," International Journal of Heat and Mass Transfer, Vol. 21, 1978, pp. 1369-1377.

5 Sparrow, E. M., Ramsey, J. W., and Altemani, C. A. C., "Experiments on In-Line Pin-Fin Arrays and Performance Comparisons with Staggered Arrays," Journal of Heat Transfer, Vol. 102, No. 1, Feb. 1980, pp. 44-50.

6 Pierson, O. L., "Experimental Investigation of the Influence of Tube Arrangement on Convection Heat Transfer and Flow Resistance in Cross Flow of Gases over Tube Banks, Transactions of the ASME, Vol. 59, 1937, pp. 563-572.

7 Huge, E. C., "Experimental Investigation of Effects of Equipment Size on Heat Convection Transfer and Flow Resistance in Cross Flow of Gases over Tube Banks," Transactions of the ASME, Vol. 59, 1937, pp. 573-581.

8 Anderson, R. C., A Microprocessor Controlled Pressure Scanning System," NASA TM X-71886, May 1976.

9 Miller, R. L., "ESCORT: A Data Acquisition and Display System for Support Research Testing," NASA TM-78909, May 1978.

10 Eckert, E. R. G., and Drake, R. M., Heat and Mass Transfer, 2nd. Edition, McGraw-Hill, New York, 1959, p. 270.

11 Hilsenrath, J., et al. Tables of Thermal Properties of Gases, NBS-Circ-564, 1955.

12 Dittus, F. W., and Boelter, L. M. K., "Heat Transfer in Automobile Radiators of the Tubular Type," University of California, Berkley, Publications in Engineering, Vol. 2 No. 13, 1930, pp. 443-461.

13 McAdams, W. H., Heat Transmission, 3rd. ed., McGraw-Hill, New York, 1954, p. 225.

14 Faulkner, F. E., "Analytical Investigation of Chord Size and Cooling Methods on Turbine Blade Cooling Requirements," AiResearch Mfg. Co., Torrance, Calif., AIRESEARCH-71-7487-BK-1, Aug. 1971, Appendix D, p. 189.

TABLE I. - PIN FIN NOMINAL GEOMETRIES

Plotting system	D_o, cm	X_T	X_S	N_T	N_L	θ, deg	Pin material
P	0.635	4	2	5	4	0	Copper
W	0.635	4	2	5	4	0	Wood
R	0.635	4	2	5	4	30	Copper
S	0.3175	2	0.5	5	4	0	Copper

TABLE II. - PLAIN CHANNEL

NOMINAL GEOMETRIES

Plotting symbol	L, cm	W, cm	H, cm
L	9.576	12.70	1.270
M	2.469	3.175	0.1588

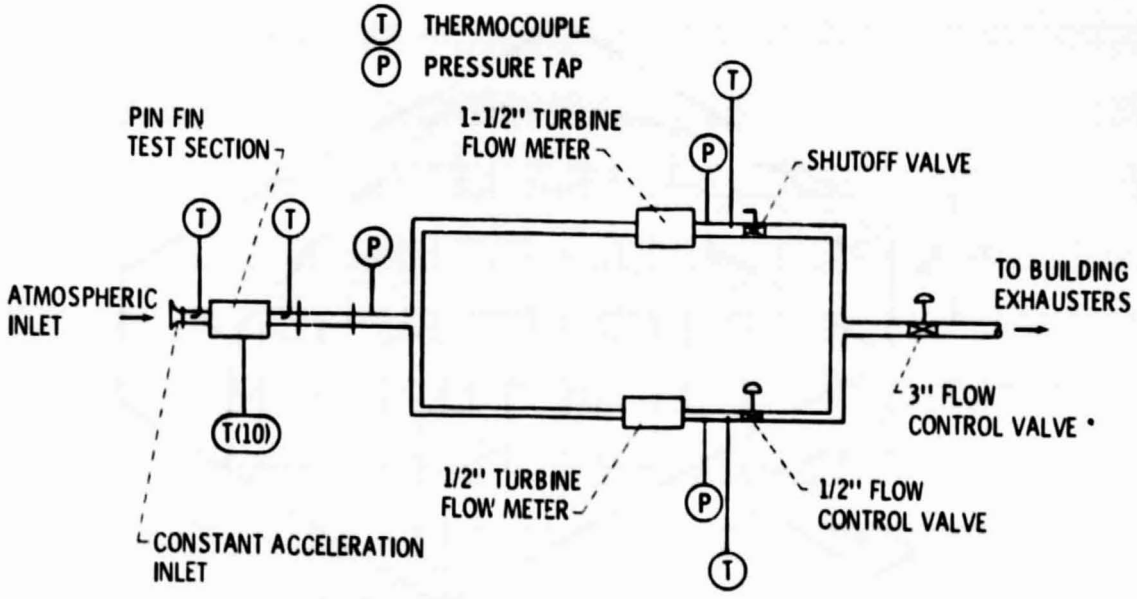

Figure 1. - Schematic of pin fin heat transfer rig.

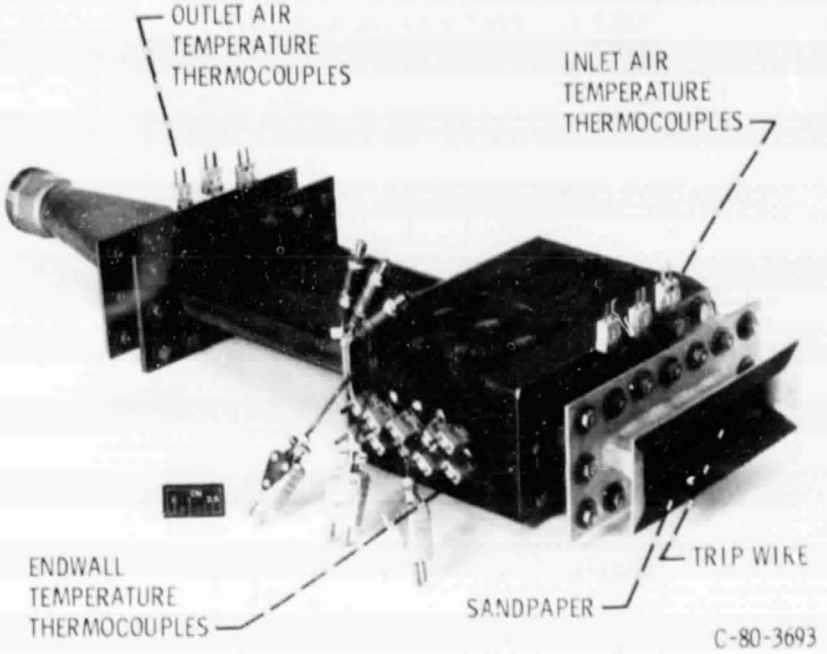

Figure 2. - Pin fin test section assembly.

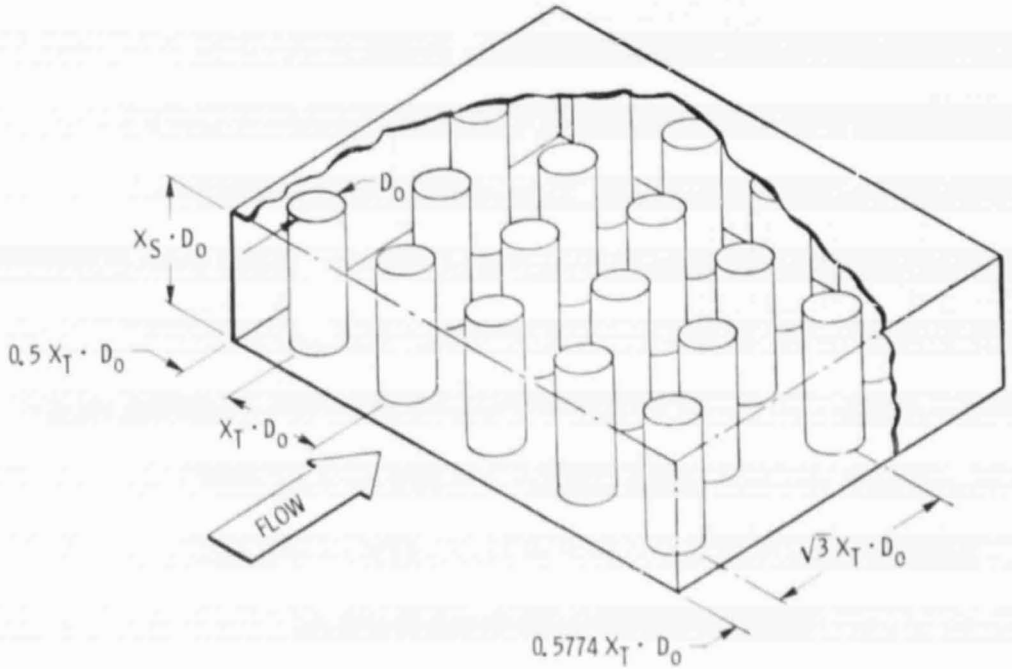

Figure 3. - Perpendicular pin fin channel geometry.

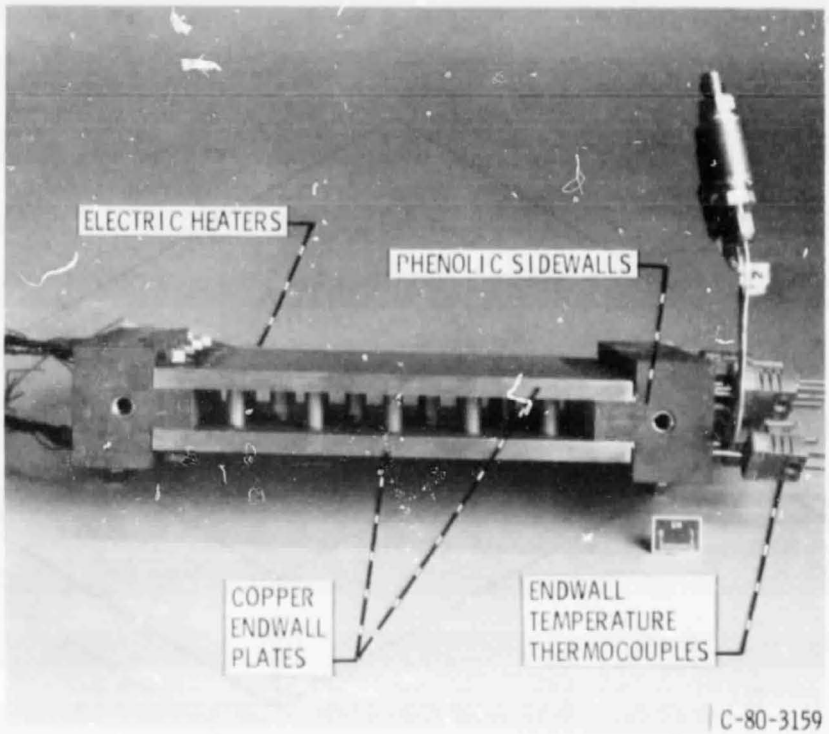

Figure 4. - Typical pin fin flow channel.

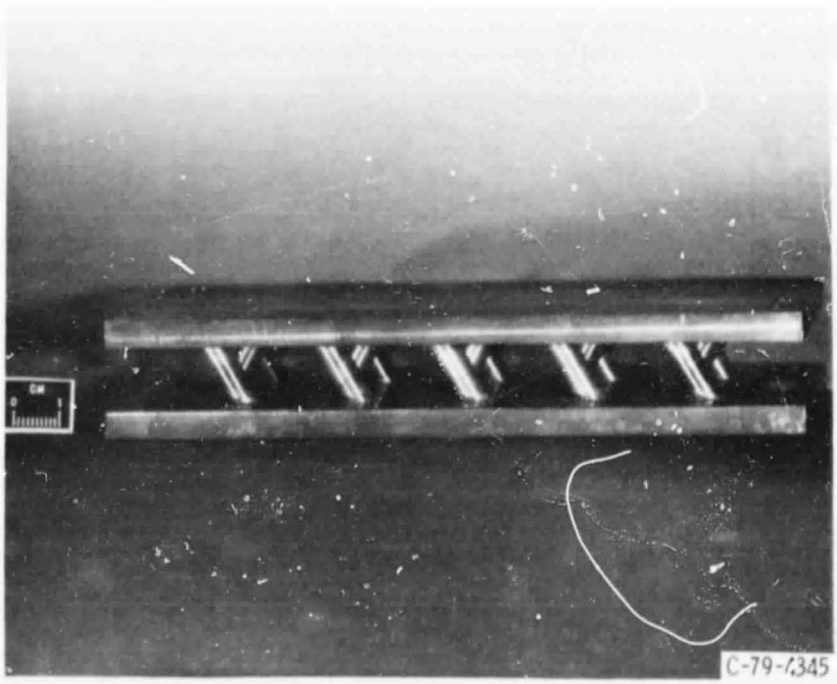

Figure 5. - Inclined pin fin flow channel.

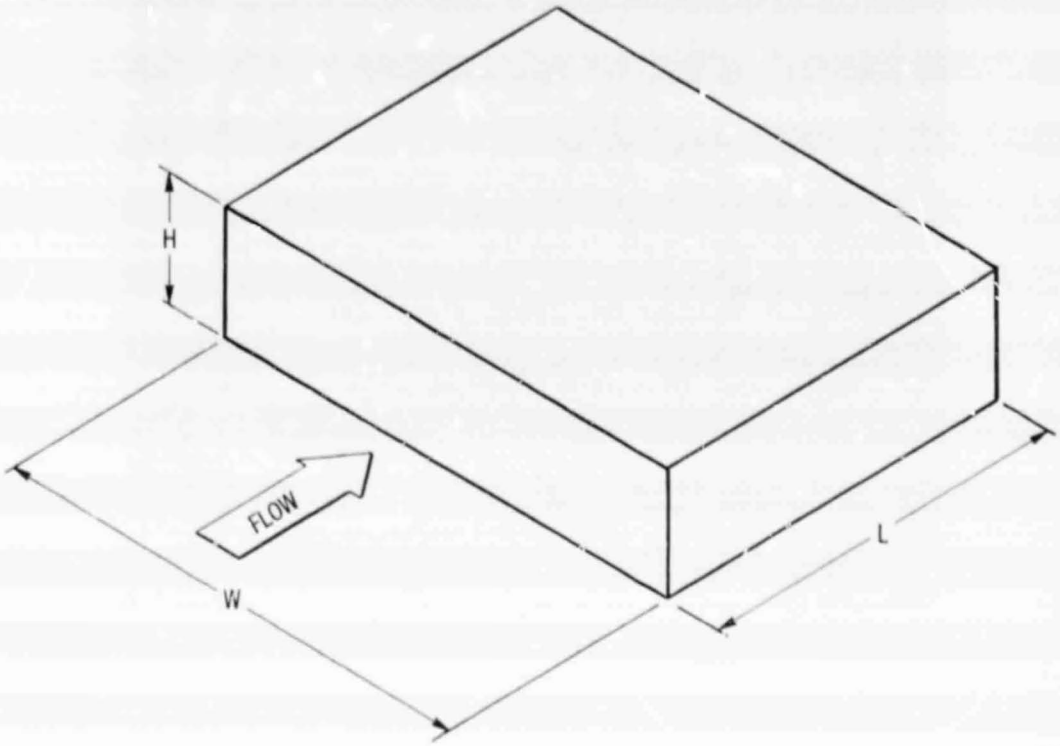

Figure 6. - Plain channel geometry.

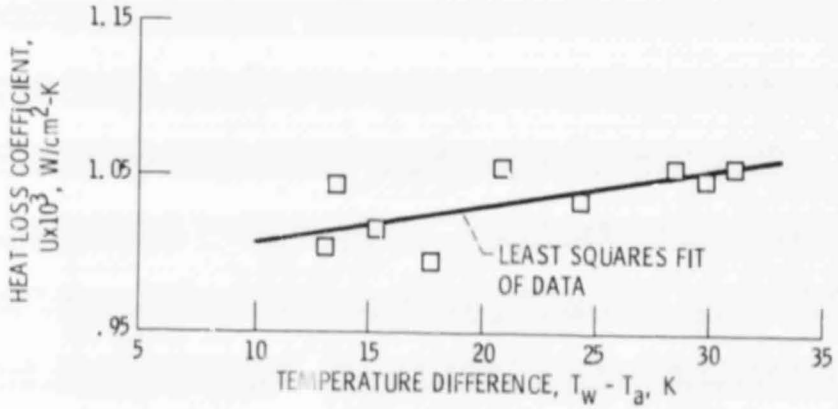

Figure 7. - Typical heat loss calibration curve.

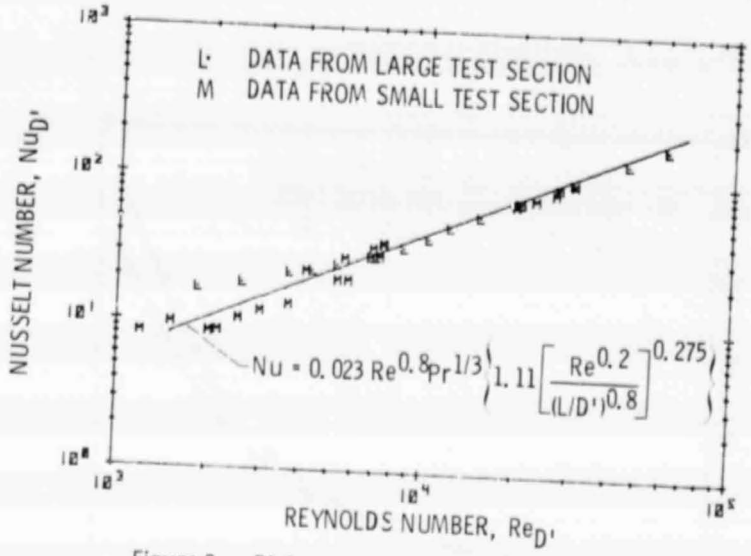

Figure 8. - Plain channel data compared to modified duct flow correlation.

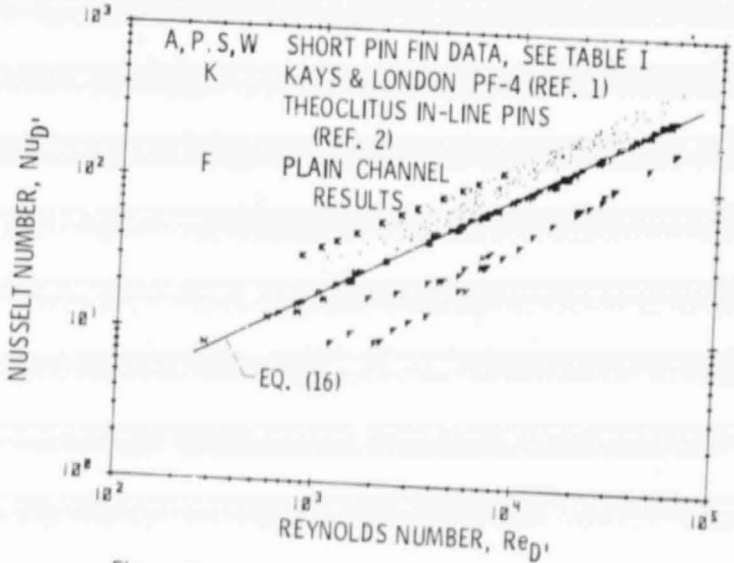

Figure 9. - Comparison of short pin fin data with long pin data and plain channel data.

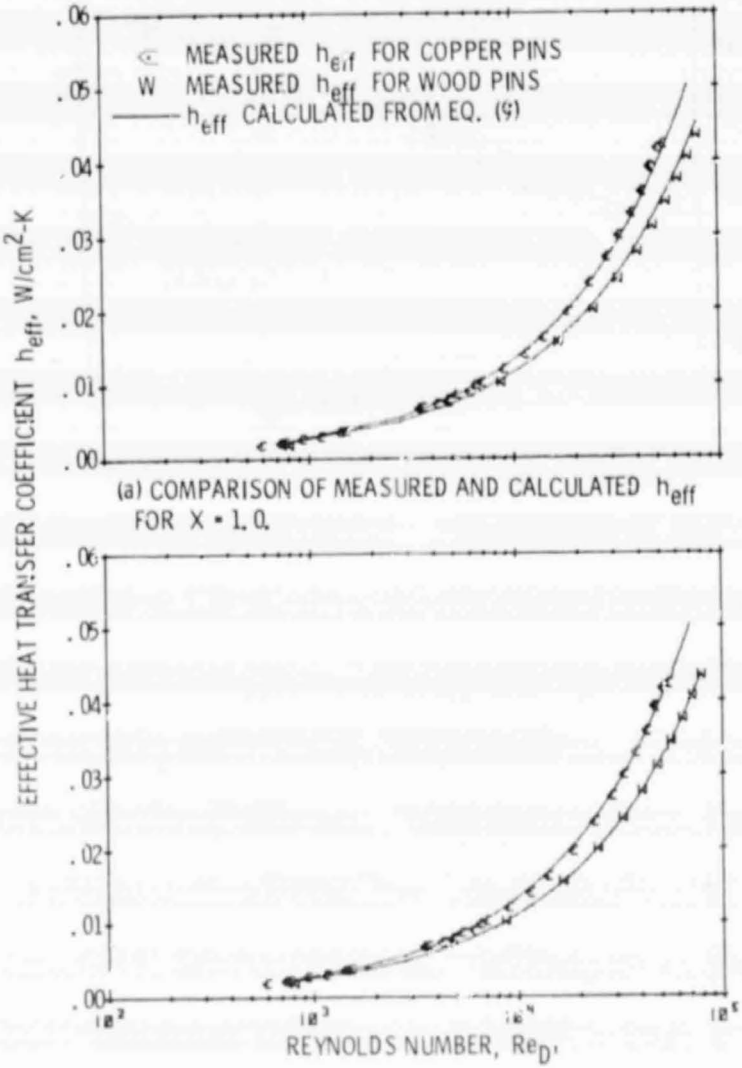

(a) COMPARISON OF MEASURED AND CALCULATED h_{eff} FOR X = 1.0.

(b) COMPARISON OF MEASURED AND CALCULATED h_{eff} FOR X = 1.3445.

Figure 10.

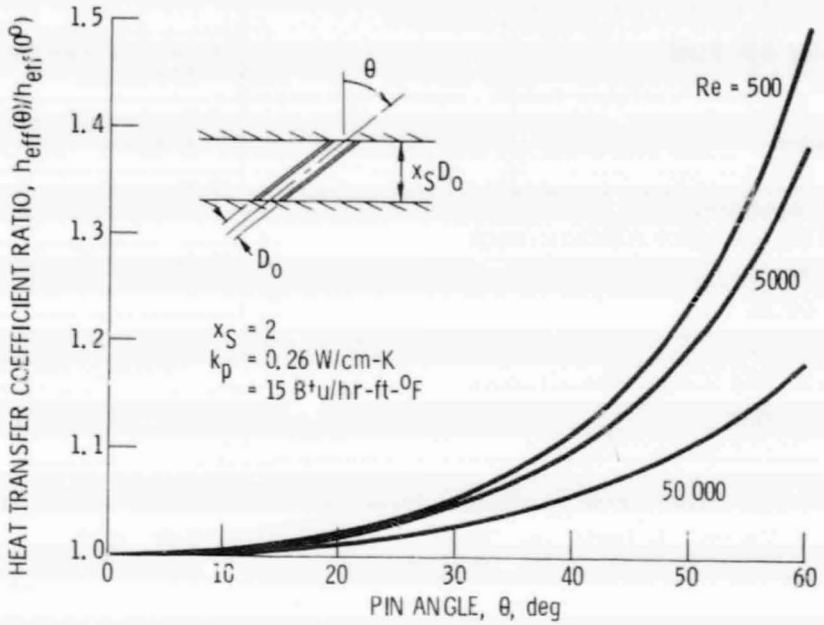

Figure 11. - Calculated increase in effective heat transfer coefficient as a function of pin angle.

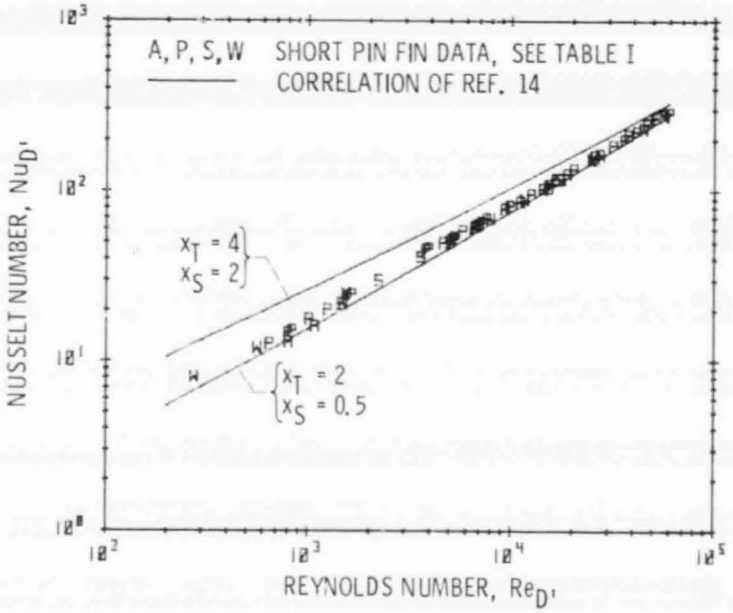

Figure 12. - Comparison of pin fin heat transfer correlation from ref. 14 with short pin fin data.